Prototype Tests of a Multiplexed Fiber-Optic Ultra Fast FADC Data Acquisition System for the MAGIC Telescope

H. Bartko, F. Goebel, R. Mirzoyan, W. Pimpl, M. Teshima
<hbartko@mppmu.mpg.de>

January 14, 2005

Abstract

Ground-based Atmospheric Air Cherenkov Telescopes (ACTs) are successfully used to observe very high energy (VHE) gamma rays from celestial objects. Light of the night sky (LONS) is a strong background for these telescopes. An ultra-fast read-out of an ACT can minimize the influence of the LONS and allows to lower the analysis energy threshold. Moreover, it could help to suppress other unwanted backgrounds.

GSamples/s flash ADCs are commercially available but are very expensive and power consuming. Here we present a novel technique of Fiber-Optic Multiplexing which uses a single 2 GSamples/s FADC to digitize 16 read-out channels consecutively. The analog signals are delayed using optical fibers. The multiplexed (MUX) FADC read-out reduces the costs by about 85% compared to using one ultra-fast FADC channel per read-out channel.

Two prototype multiplexers, digitizing data from 32 channels, have been built and tested. The ultra fast read-out system will be described and the test results will be reported. The new system will be implemented as a full scale read-out for the MAGIC telescope.

Contents

1 Introduction

MAGIC is the world-wide largest Imaging Air Cherenkov Telescope (IACT) aiming to study gamma ray emission from the high energy phenomena and the violent physics processes in the universe at the lowest energy threshold amongst the existing IACTs. An overview about the gamma ray astronomy with IACTs is given in [1]. MAGIC is a unique detector that will cover the energy range / energy gap between the gamma ray satellite missions and other ground-based Cherenkov telescopes [2].

The camera of the MAGIC Telescope consists of 576 Photomultiplier tubes (PMTs), which deliver about 2 ns FWHM fast pulses from gamma ray induced air showers. The currently used read-out system [3] is relatively slow (300 MSamples/s). To acquire the pulse shape an artificial pulse stretching to about 6.5 ns FWHM is used. Thereby also more light of the night sky is integrated that acts as noise. This limits the analysis energy threshold of the telescope and reduces the selection efficiency of the gamma signal from different backgrounds.

For 2 ns FWHM fast pulses a 2 GSamples/s FADC provides at least 4 sampling points. This permits a reasonable reconstruction of the pulse shape and could provide an improved gamma/hadron separation based on timing. The ultra fast read-out can strongly improve the performance of MAGIC. The improved sensitivity and the lower analysis energy threshold will considerably extend the observation range of MAGIC and allows to search for very weak sources at high red shifts.

A few GSamples/s flash ADCs are commercially available but are very expensive and power consuming. To reduce the cost of an ultra-fast read-out system, at the Max-Planck-Institut für Physik in Munich a 2 GSamples/s read-out system has been developed using the novel technique of Fiber-Optic Multiplexing. The new technique uses a single 2 GSamples/s FADC to digitize 16 read-out channels consecutively. The analog signals are delayed by using optical fibers. A trigger signal is generated using a fraction of the light which is branched off by fiber-optic light splitters before the delay fibers. With the Fiber-Optic Multiplexing a cost reduction by about 85% can be achieved compared to using one 2 GSamples/s FADC per read-out channel.

The suggested 2 GSamples/s multiplexed (MUX) FADC system will have a 10 bit amplitude resolution. For large signals the arrival time of the Cherenkov pulse can be determined with a resolution better than 200 ps. The system is relatively simple and reliable. All optical components and the FADCs are commercially available, while the multiplexer electronics has been developed at the MPI in Munich. Two prototype multiplexers, for 32 channels in total, have been built and tested in-situ as read-out of the MAGIC telescope in La Palma in August 2004.

In section 2 the MAGIC experiment is briefly described in the context of the data acquisition (DAQ) system using ultra-fast FADCs. The specifications of the ultra-fast read-out are described in section 3, followed by the measured performance for the MUX-FADC prototype in laboratory tests (section 4) and as read-out of the MAGIC telescope (section 5). Section 6 is dedicated to discussions and conclusions. Finally, section 7 gives an outlook to the planned final setup of the MUX-FADC system as a read-out of the MAGIC telescope.

2 Principle and Signal Processing of the MAGIC Telescope

Since the details of the MAGIC telescope are described elsewhere [4], only items relevant to the FADC system are presented in this section. Figure 1 shows the working principle of MAGIC. A high energy gamma ray entering the earth's atmosphere initiates a shower cascade of electrons and positrons. These radiate Cherenkov light, which is collected by the mirror and focussed onto the PMT camera of the MAGIC telescope. The main background originates from much more frequent showers induced by hadronic cosmic rays.

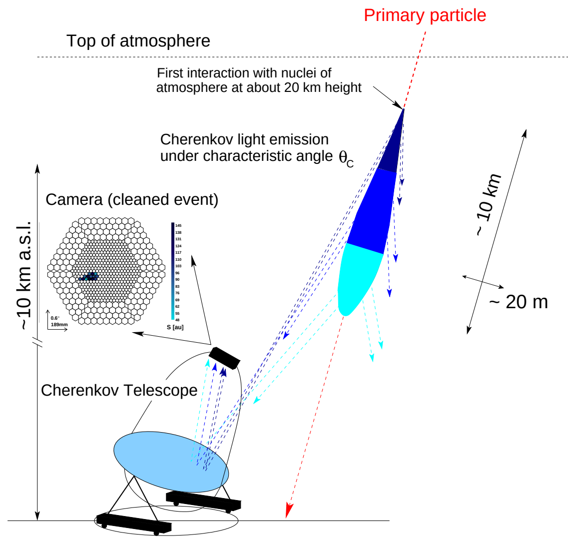

Figure 1: IACT principle: A cosmic high energy gamma ray penetrates the earths atmosphere and initiates a shower cascade of electrons and positrons, which radiate Cherenkov light. This light is collected and focussed onto the camera providing an image of the air shower. Picture taken from [5].

Monte Carlo (MC) based simulations predict different time structures for gamma and hadron induced shower images as well as for images of single muons. The timing information is therefor expected to improve the separation of gamma events from the background events. Figure 2 shows the mean amplitude (a, c) and time (b, d) profiles for gamma (c, d) and hadron (a, b) induced air showers. The impact parameter is fixed to 120 m and the initial gamma energy is set to 100 GeV, while the proton energy is set to 200 GeV. The profiles are obtained by averaging over many simulated showers [6]. The timing structure of the image can provide viable information about the head and the tail of the shower as well as a discriminant between gamma and hadron induced showers.

The MAGIC read-out chain, including the PMT camera, the analog-optical link, the majority trigger logic and FADCs, is schematically shown in figure 3. The used PMTs provide a very fast response to the input light signal. The response of the PMTs to sub-ns input light pulses shows a FWHM of 1.0 - 1.2 ns and rise and fall times of 600 and 700 ps correspondingly [7]. By modulating vertical cavity surface emitting laser (VCSEL) diodes in amplitude the ultra fast analogue signals from the PMTs are transferred via 162m long, multimode graded index 50/125 μm diameter optical fibers to the counting house [8]. After transforming the light back to an electrical signal, the original PMT pulse has a FWHM of about 2.2 ns and rise and fall times of about 1ns.

In order to sample this pulse shape with the used 300 MSamples/s FADC system, the pulse is stretched to a FWHM $>$ 6 ns (the original pulse is folded with a stretching function of 6ns). This implies a longer integration of LONS and thus the performance of the telescope on the analysis level is degraded.

Because the current MAGIC FADCs have a resolution of 8 bit only, the signals are split into two branches with a factor of 10 different gains. One branch is delayed by 55 ns and then both branches are multiplexed and consecutively read-out by one FADC. The FADC system can be read out with a maximum sustained rate of 1 kHz. A 512 kbytes FIFO memory allows short-time trigger rates of up

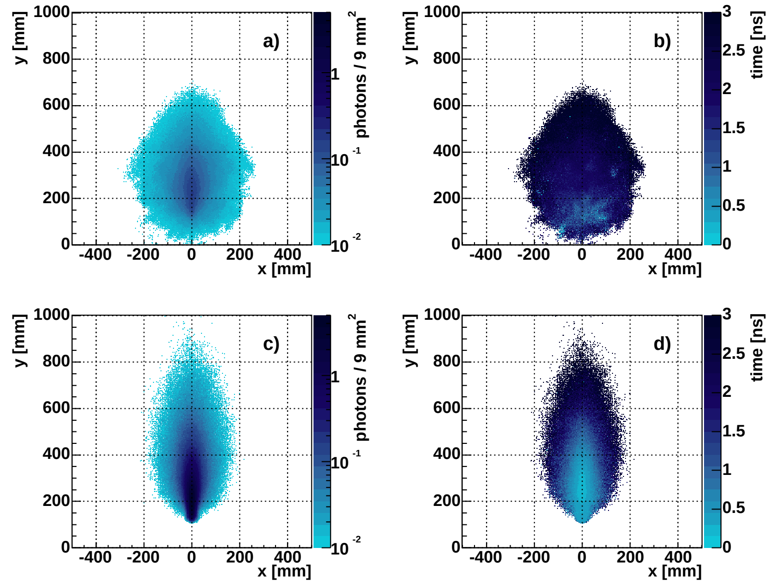

Figure 2: Mean amplitude (a, c) and time (b, d) profiles for gamma (c, d) and hadron (a, b) induced air showers from MC simulations. The impact parameter is fixed to 120 m and the initial energy of the gamma is set to 100 GeV, while the proton energy is set to 200 GeV. The profiles are obtained by averaging over many simulated showers [6]. The timing structure of the image can provide viable information about the head and the tail of the shower as well as a discriminant between gamma and hadron induced showers.

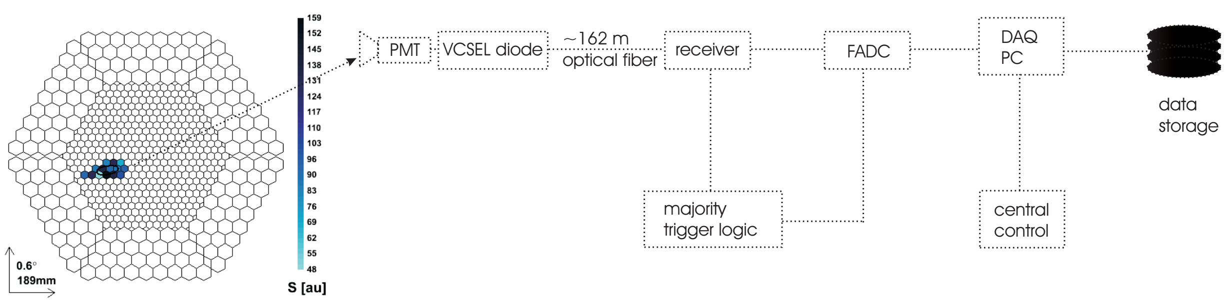

Figure 3: Current MAGIC read-out scheme: the analog PMT signals are transferred via an analog optical link to the counting house where after the trigger decision the signals are digitized by using a 300 MHz FADCs system and written to the hard disk of a DAQ PC.

to 50 kHz.

3 The Ultra Fast Fiber-Optic MUX-FADC Data Acquisition System

The MAGIC collaboration intends to improve the performance of its telescope by installing a fast ≤ 2 GSamples/s FADC system which fully exploits the intrinsic time structures of the Cherenkov light pulses. The requirements for such a system are the following:

- 10 bit resolution at a 2 GSamples/s sampling rate
- ≥ 500 MHz bandwidth of the electronics chain including the FADC
- up to 1 kHz sustained event trigger rate
- dead time $\leq 5\%$.

3.1 General MUX-Principle

It is interesting to note that in experiments where FADCs are used to read-out a multichannel detector in the common event trigger mode, only a tiny fraction of the FADC memory depth is occupied by the signal while the rest is effectively "empty" [9, 10]. One can try to correct this "inefficiency of use" by "packing" the signals of many channels sequentially in time into a single FADC channel, i.e. by multiplexing.

Following this general idea a multiplexing system with fiber-optic delays has been developed for the MAGIC telescope. The block diagram is shown in figure 4.The ultrafast fiber-optic multiplexer consists of three main components:

- fiber-optic delays and splitters
- multiplexer electronics: fast switches and controllers
- ultra fast FADCs.

After the analog optical link between the MAGIC PMT camera and the counting house the optical signals are split into two parts. One part of the split signal is used as an input to the trigger logic. The other part is used for FADC measurements after passing through a fiber-optic delay line of a channel-specific length.

The multiplexer electronics operate in the following way: The common trigger from the majority logic unit opens the switch of the first channel and allows the analog signal to pass through and be digitized by the FADC. All the other switches are closed during this time. When the digitization window for the first channel is over the corresponding switch is closed. The closed switch strongly attenuates the signal transmission by more than 50 dB for the fast MAGIC signals. Then the switch number two is opened such that the accordingly delayed analog signal from the second channel is digitized and so forth, one channel at a time until the last one is measured. In this way one "packs" signals from different channels in a time sequence which can be digitized by a single FADC channel.

Because of the finite rise and fall times of the gate signals for the switches and because of some pick-up noise from the switch one has to allow for some switching time between the digitization of two consecutive channels. The gating time for each channel has been set to 40 ns, of which the first and last 5 ns are affected by the switching process.

For the use in MAGIC a $16 \rightarrow 1$ multiplexing ratio has been chosen. 16 channels are read-out by a single ultra fast FADC channel. The chosen multiplexing ratio is a compromise between

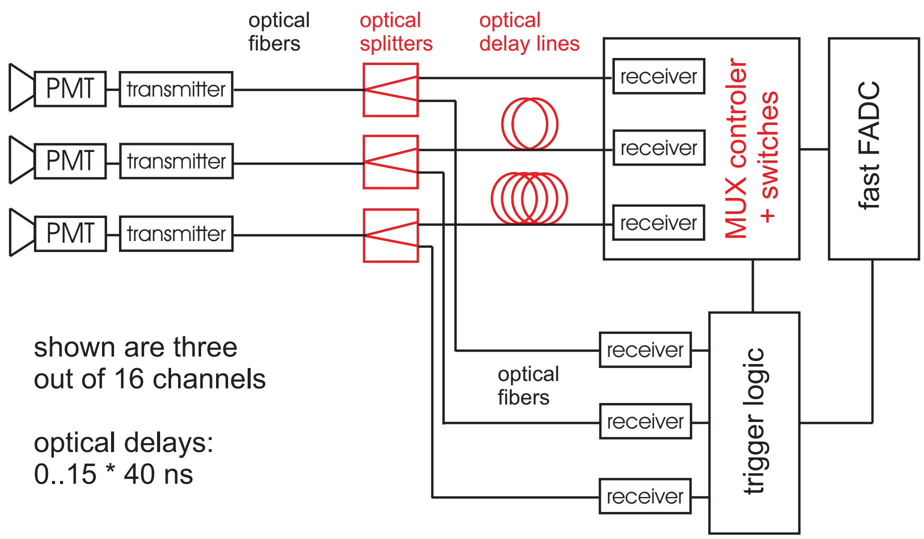

Figure 4: Schematic diagram of the multiplexed fiber-optic ultra fast FADC read-out. Part of the analog signal that arrives via the fiber-optic link from the PMT camera is branched of and fed into a majority trigger logic. The other part of the signals is consecutively delayed in optical fibers. One channel after the other is connected to the ultra fast FADC using fast switches. Thereby the noise from the other channels is efficiently blocked.

- Dead time: The digitization of one event takes 16*40 ns=640 ns. During this time no other event can be recorded. Compared to the maximum sustained trigger rate of up to 1 kHz this dead time is acceptable.
- Noise due to cross-talk through the closed switches: The attenuated noise of the other channels could influence the active signal channel.
- Cost of the FADCs
- Mechanical constraints, e.g. board size, wire length.

3.2 Optical Delays and Splitters

Optical fibers have been chosen for the analog signal transmission between the PMT camera and the counting house because they are lightweight, compact, immune to electro-magnetic pick-up noise and provide no pulse dispersion and attenuation [8]. The signal attenuation at 1 km fiber length is about 2.3 dB for the chosen 850 nm wavelength of the VCSELs. The analog signal transmission offers a dynamic range larger than 60 dB.

Using fiber-optic delays ultra-fast analog signals can be delayed by several hundreds of ns. Thus a large number of successively delayed signals can be multiplexed and read out by a single channel FADC. Part of the analog signal has to be split off before the delay lines in order to initiate the coincidence trigger. Therefore fiber-optic splitters of type $1 \rightarrow 2$ of a specified ratio are used.

Figure 5 shows a module containing two optical delay lines of 142 m and 150 m length, corresponding to a delay of 710 ns and 750 ns. Figure 6 shows a module of four GRIN-type fiber-optic splitters with 50:50 splitting ratio (for a technical description see [11]). The modules have standardized outer dimensions and can be assembled in 3U hight 19" crates. The splitters and optical delay lines are commercially available from the company Sachsenkabel [12].

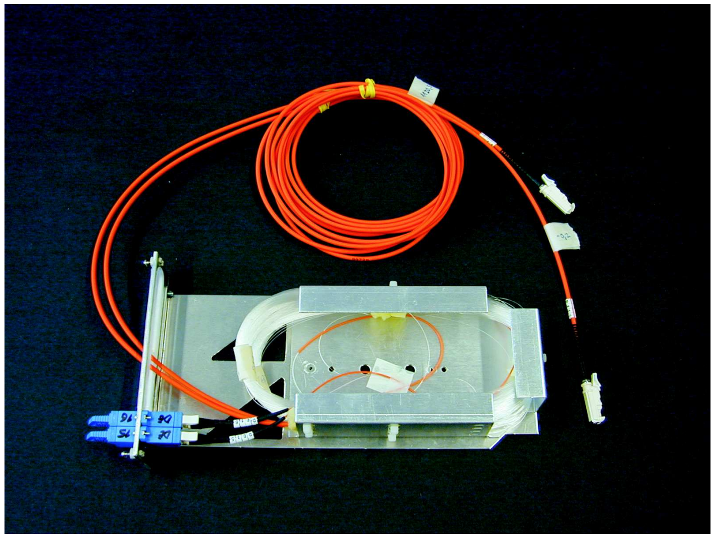

Figure 5: Two channel fiber-optic delay module of 142 and 150 m length, corresponding to a delay of 710 and 750 ns, respectively. Mechanical dimensions: 235 mm * 130 mm (3U) * 35 mm (7HP).

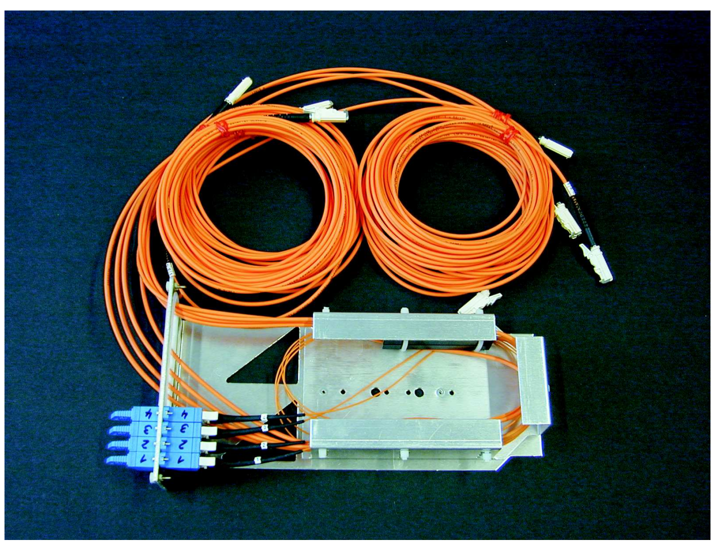

Figure 6: Four channel fiber-optic splitter module, GRIN technology and 50:50 splitting ratio. The outer dimensions are: 235 mm * 130 mm (3U) * 35 mm (7HP).

3.3 MUX Electronics

The multiplexer electronics consist of four stages. The first stage is a fiber optic receiver, where the signals from the optical delay lines are converted back to electrical pulses using PIN diodes. In a second stage, part of the electrical signal is branched off and transferred to a monitor output. The third stage consists of ultra fast switches which are activated one at a time. In the last stage all 16 channels are summed to one output. The multiplexed signals are then transferred via 50 Ω coaxial cables to the FADC channels. Table 1 summarizes the specifications of the multiplexer electronics.

Mechanical size	370 mm (9 U) * 220 mm * 30 mm (6 HP)
Number of channels	16
Analog input	via 50/125 μm graded index fiber, E2000 connector
Gain	50, including the VCSEL transmitter
Dynamic range	max output amplitude: 1 V
Power supplies	+12 V, ±5 V
Power dissipation	20 W
Trigger input	LVDS

Table 1: Specifications of the electronics for analog signal multiplexing.

One multiplexer module consists of one 6 layer *motherboard* and 16 double layer *switchboards*, which are plugged into the *motherboard* via multiple pin connectors. Figure 7 shows a photo of the printed circuit MUX *motherboard* with 16 mounted daughter *switchboards*.

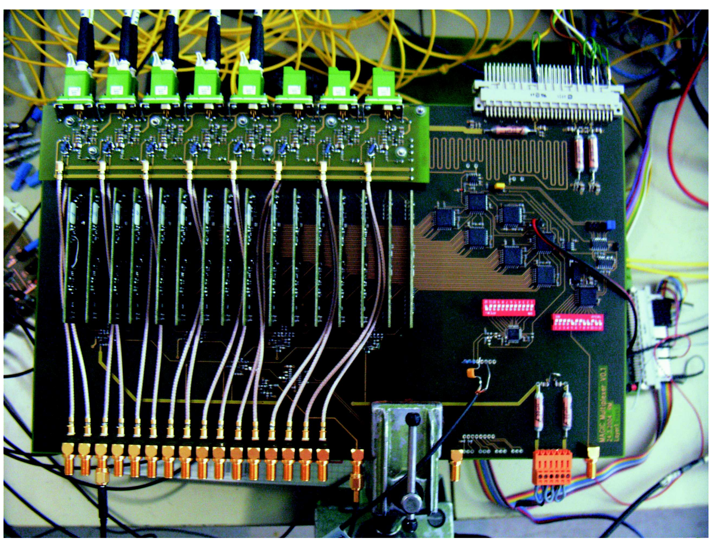

Figure 7: Photo of the printed circuit board for analogue signal multiplexing: It consists of a trigger input, 16 opto-electric converters, 16 monitor signal outputs, the Digital Switch Control circuit (DSC), 16 daughter switch boards and two summing stages. The overall size is 370 mm (9 U) * 220 mm * 30 mm (6 HP). – picture to be updated, latest production prototype, black background –

The *motherboard* includes the following components:

- 16 opto-electrical converters
- 16 monitor outputs
- the Digital Switch Control circuit (DSC)
- trigger input to activate the DSC
- 16 ultra-fast switches on 16 *switchboards*
- the 16 channel summing stage.

One opto-electrical converter consists of a receptacle, a PIN photo diode, packed in the E2000-connector. The photodiode is biased by 12 V to reduce its intrinsic capacity for speed and noise optimization. The current signal of the PIN photo diode is converted into an equivalent voltage signal by a transimpedance-amplifier. Its amplifier-IC has a gain-bandwidth product of about 1.5 GHz and a very high slew rate of about 4000 V/μs. The trans-impedance is 1000 Ω. A monitor output consists of an ultra-wide band (UWB)-driver-amplifier, which transmits the signal from the transimpedance-stage to a 50 Ω-SMA-connector.

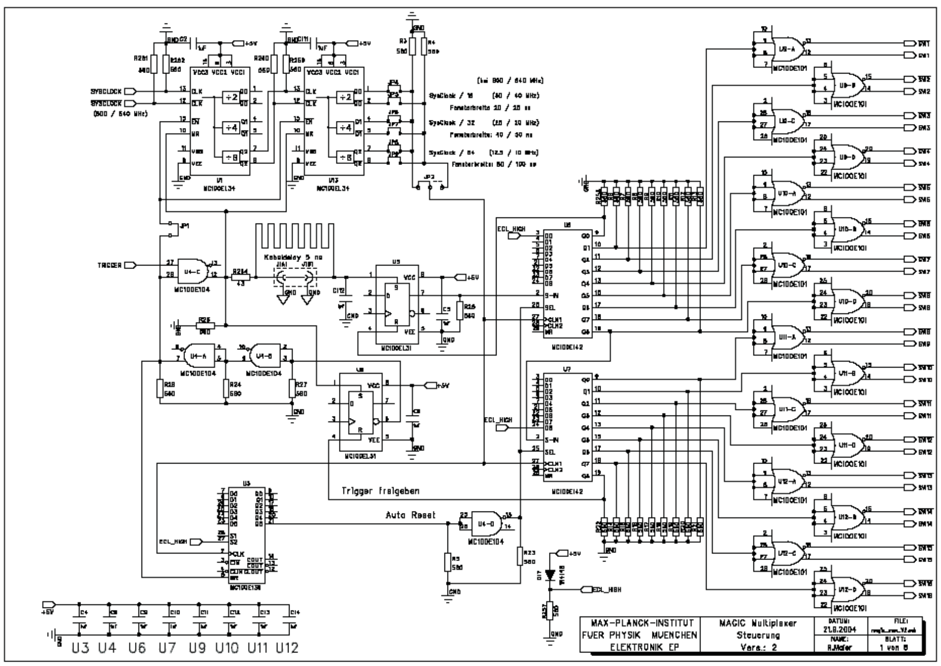

Figure 8: Circuit diagram of the Digital Switch Control circuit (DSC): The trigger initiates a sequence of 16 PECL high levels of 40 ns duration applied consecutively to the switch boards.

Figure 8 shows the circuit diagram of the Digital Switch Control circuit, DSC. It consists of the following parts:

- One clock generator-IC. It is programmable with a resolution of 12 bit from 50 MHz to 800 MHz and works in PECL mode. It is crystal stabilized and set to 800 MHz.

- A digital delay line (DDL) that can be set from 2 ns to 10 ns with 11 bit accuracy. It can be used to adjust the trigger times between different MUX *motherboards*.
- A digital lock-in-circuit (DLC) synchronizes the MUX-sequence to the trigger signal. The lock-in jitter is 1.25 ns (= 1/800 MHz).
- 16 differential PECL-drivers that transmit the MUX-sequence signals to the corresponding *switchboards*.

Each switchboard includes two ultra-wideband (UWB)-amplifier circuits, followed by two ns-switching MOSFETs operated in series and one UWB-driver-amplifier-circuit. MOSFET switches have been chosen due to their fast switching properties and a very fast stabilization of the signal baseline after the switching. The small cross-talk through the closed switch is further reduced by the serial operation of two switches. An on-board PECL to CMOS converter distributes the digital switch-control-circuit (DSC)-signal to the MOSFET-switches in parallel. Figure 9 shows a photo of the switch board, while its circuit diagram is shown in figure 10.

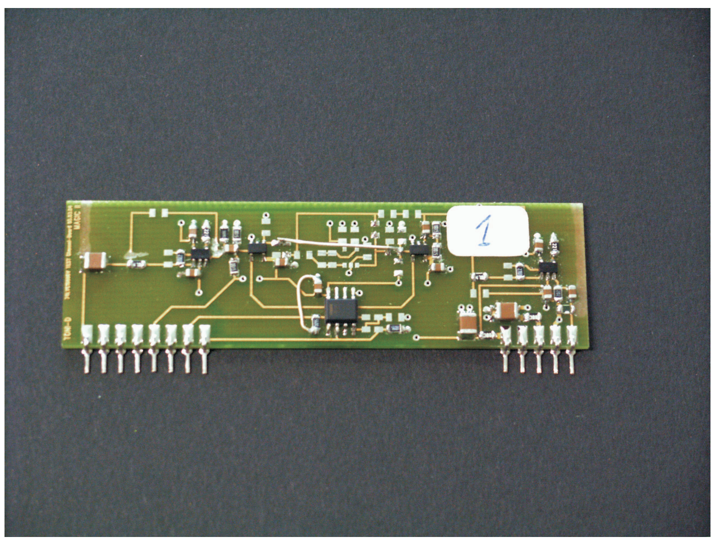

Figure 9: The printed circuit board for fast switching. The switch board contains two ns-MOSFET-switches operated in series. Its mechanical dimensions are 80 mm * 20 mm *5 mm. – picture to be updated, latest production prototype –

In a passive summation the switch output capacitances would sum up and significantly widen the signal pulse. To get rid of this effect a two step active summation has been chosen: In the first step, the outputs of four channels are summed together. In the second step the obtained four outputs are summed to one. For the summing also UWB-amplifiers are used. The two-step-setup keeps the channel-wires short and allows to use the amplifiers in the faster inverting mode while keeping the signal polarity non-inverting. Finally, an UWB-driver sends the multiplexed signals over a 50 Ω-SMA-coaxial connection to the FADC. The circuit diagram of the summation stage is shown in figure 11.

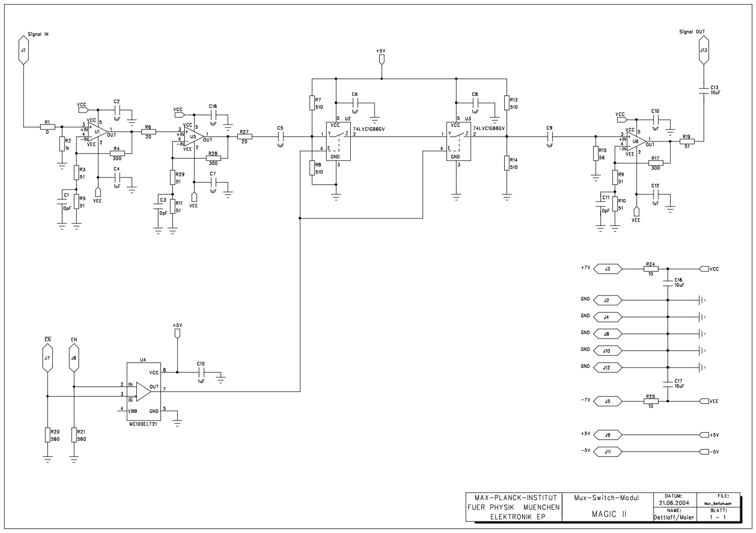

Figure 10: Schematics of the fast switches: A high PECL level from the Digital Switch Control circuit opens both of the ns-MOSFET switches operated in series.

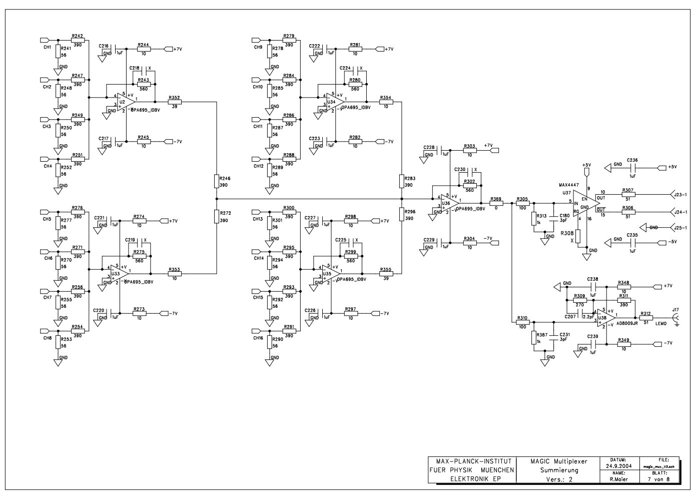

Figure 11: Schematics of the two step summing stage of the multiplexed signals. The two-step-setup keeps the channel-wires short and allows to use the UWB-amplifiers in the faster inverting mode while keeping the signal polarity non-inverting.

3.4 FADC Read-Out

The FADCs are commercial products manufactured by the company Acqiris (DC 282) [13]. They feature a 10 bit amplitude resolution, a bandwidth of 700 MHz, a sampling speed of 2 GSamples/s and an input voltage range of 1 V. Each FADC board contains 4 channels. The read-out data are stored in a RAM on the FADC board of 256 kSamples (512 kbytes) size per channel. Up to 4 FADC boards can be arranged in one compact PCI crate and are read-out by a crate controller PC running under Linux. The FADCs are designed for a 66 MHz 64 bit data transfer via the compact PCI bus.

The FADC features a trigger time interpolator TDC that can be used to correct for a potential trigger jitter of 500 ps due to the asynchronous FADC clock with respect to the trigger decision. Table 2 summarizes the specifications of the ultra-fast FADCs.

Mechanical size	267 mm (6 U) * 220 mm * 30 mm (6 HP)
Number of channels	4
Analog input	1 V full scale, adjustable offset
Sampling frequency	2 GSamples/s
Sampling resolution	10 bits
RAM size	256 kSamples (512 kbytes) per channel
Bandwidth	700 MHz
Noise level	$<$ 1.2 LSB guaranteed
Power dissipation	60 W (4 channels)
Trigger input	unipolar, adjustable threshold

Table 2: Specifications of the ultra-fast FADC.

4 Performance of the System Components

The performance of the MUX-FADC system components has been studied in extensive laboratory tests. The quality and performance of the FADCs and of different commercially available optical splitters and delays have been evaluated. Several iterations of the multiplexer electronics design have been made.

4.1 Performance of the Optical Delays and Splitters

The fiber optic delay lines have channel specific delay times of 0...15 times 40 ns plus 500 ns common base delay. Deviations from the specified delay times and potential changes in the delay due to temperature variations are important. It has to be ensured that all signals arrive in time at the multiplexer electronics when a given switch is open.

Figure 12 shows the distribution of the differences between the measured delay times and the nominal channel specific ones. On average the measured delay lengths coincide with the nominal ones with an RMS deviation of about 2 ns.

For the selected wavelength of the VCSEL diodes of 850 nm the attenuation of the signals in the used graded index fiber is only about 3 dB/km. Nevertheless there are small differences in the dispersion of the signals due to the different delay lengths from channel to channel. Figure 13 shows the signal attenuation as a function of the measured delay length. The signal attenuation coefficient $A = 20\log_{10}(S_0/S)\mathrm{dB}/\Delta t$, where S_0 is the signal before the delay and S the signal after the fiber-optic delay of delay time Δt, is determined to be:

$$A = (1.8 \pm 0.1)\ \mathrm{dB}/\mu\mathrm{s}\ . \tag{1}$$

Different technologies of fiber-optic splitters are available on the market. Three splitting technologies have been tested: fused splitters, bifurcation splitters and so called GRIN-splitters. In the fused

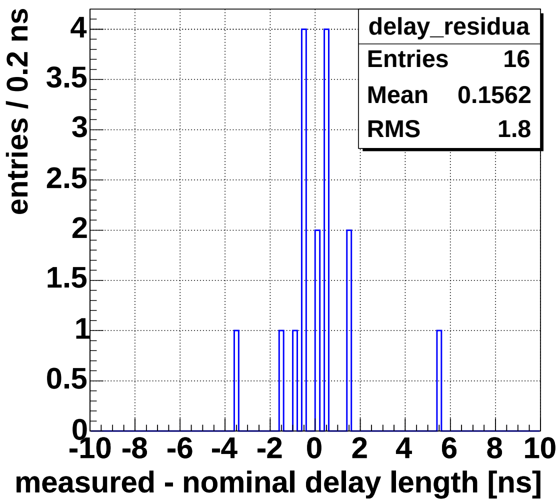

Figure 12: Distribution of the measured deviations of the fiber delay times from the specified channel specific delay of 0...15 ns plus common base delay. – figure to be updated with the results of 600 delays –

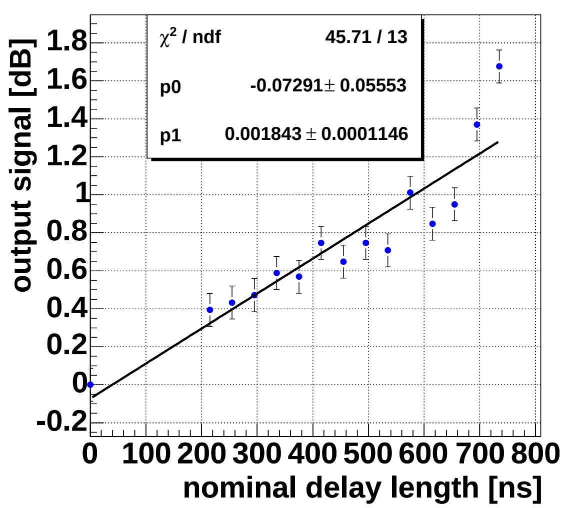

Figure 13: Signal Attenuation in the optical delay lines. The signal attenuation coefficient is determined to be (1.8 ± 0.1) dB/μs.

technology two optical fibers are drilled and then thermally fused together. In bifurcation splitters the end faces of the two output fibers are mechanically attached to the end face of the input fiber. In GRIN-type splitters the splitting is done by a semi-transparent mirror in conjunction with two graded index lenses [11].

The splitting ratio is guaranteed to be 50:50 within ± 3 % by the manufacturer. All tested splitters have been found to be insensitive with respect to time and temperature changes.

The MAGIC optical link uses multimode VCSELs and multimode optical fibers. Mechanical stress or deformations of the input fiber into the splitter, especially due to telescope movements, can vary the light modes in the fiber. The expected movements of the fibers have been simulated in the laboratory by bending the fibers using different bending radii. The fused and bifurcation fiber optic splitters show changes in the splitting ratio of more than ± 10 %. Only the so called GRIN type splitters are immune against mode changes, with changes of the splitting ratio of less than 1% for them.

Figure 14 shows the distribution of the measured deviations of the fiber-optic splitters from the specified 50:50 splitting ratio. The distribution is centered around zero and has an RMS of about 1.5 %.

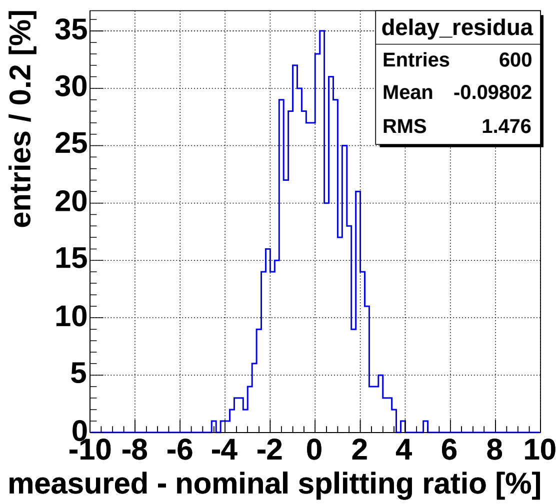

Figure 14: Distribution of the measured deviations of the GRIN-type fiber-optic splitters from the specified 50:50 splitting ratio. – figure to be updated with the results of all 352 GRIN-splitters –

4.2 Performance of the MUX Electronics

The MUX electronics have been extensively tested in the laboratory. For the use as a read-out for MAGIC the following points are very important:

- short switching noise and flat signal base-line
- high bandwidth (low pulse dispersion in amplitude and time)
- strong signal attenuation for closed switches
- good linearity and large dynamic range
- stability.

Figure 15 shows a photo recorded with a fast oscilloscope of two consecutively multiplexed signals along with the switching noise between two channels. Although the switching noise is as large as 100

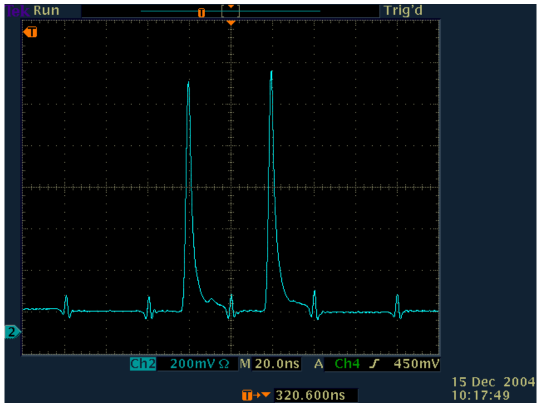

Figure 15: Oscilloscope photo of two consecutive multiplexed signals and the baseline of two empty signal gates.

mV, it is very stable and confined to less than 10 ns of the 40 ns window per read-out channel. In the rest of the window the baseline is flat and stable.

The switching and summing stages only moderately widen the fast input pulses. A pulse of about 2.5 ns FWHM after the receiver photo diode is widened to 2.7 ns FWHM at the output of the multiplexer electronics. The pass-through of such fast signals through closed switches is less than 0.5% corresponding to an attenuation of the out of time noise by about 50 dB.

Figure 16a shows the combined linearity of the switches and of the summing stage. The output signal amplitude of the MUX-board is plotted as a function of the input signal amplitude after the PIN-Diode, as measured at the monitor output. The right panel of the figure shows the deviations from linearity of the MUX-electronics. For output signals up to 1 V the MUX-electronics is linear with deviations less than 2%.

4.3 FADC Performance

The main performance parameters of the FADC are

- noise level
- linearity and bandwidth
- maximum trigger and acquisition rate
- dead time.

A noise level of less than 1.2 least significant bits (LSBs) is guaranteed by the manufacturer (700 MHz bandwidth, no input amplifier). There are small but constant differences in the input voltage full scales and thus in the gain for different FADC channels. These can be corrected for by the offline calibration software. The FADCs feature an internal calibration system keeping their integral and differential non-linearity below one LSB.

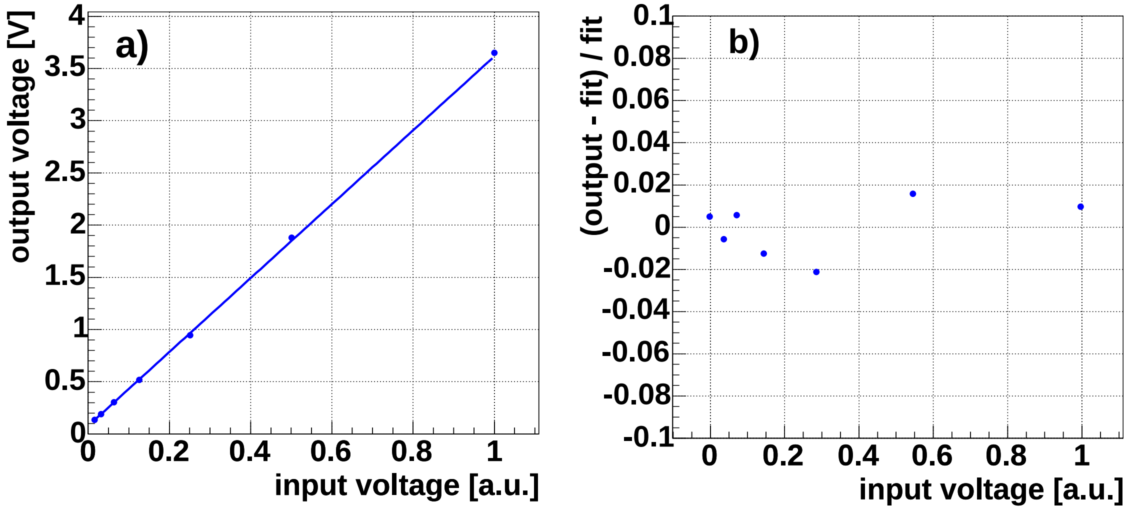

Figure 16: a) Output signal amplitude of the MUX board as a function of the input signal after the PIN diode as measured at the monitor output. b) Residua of the linearity of the MUX board as a function of the input signal after the PIN receiver diode as measured at the monitor output. The deviations are less than 2%. – plots to be updated, last production prototype of the MUX board, 3dB steps, log scale –

For the maximum trigger rate and the dead time optimization the interplay between the FADC boards and the crate controller PC is important. The compact PCI bus allows an effective data throughput of 80-100 Mbytes/s (33 MHz, 32 bit) up to about 400 Mbytes/s (66 MHz, 64 bit) shared between all FADC channels in one crate.

In each event 2560 samples are acquired per FADC channel (16 channels of 40 ns gate time, 2 GSamples/s and 2 bytes per sample for the 10 bit resolution FADC). Reading out 8 FADC channels with one crate controller board results in a data volume of about 20 kbytes/event, which has to be transferred via the cPCI bus.

The ultra-fast FADC offers three modes of data acquisition:

- single acquisition
- segmented memory
- asynchronous acquisitions using a FIFO memory.

In the single acquisition mode the digitizer acquires one waveform of $N = 1280$ samples. The crate controller CPU then uses direct-to-memory access (DMA) to the FADC RAM and reads the FADC data via the cPCI bus. Thereafter the CPU rearms the trigger for the next data acquisition. The read-out time T_1 per event and per FADC channel in the crate is given by the sum of the DMA overhead time, $\mathrm{Ovhd_{DMA}} \leq 25\mu$s and the data transfer time over the cPCI bus [13]:

$$T_1 = \mathrm{Ovhd_{DMA}} + N \cdot 2\mathrm{bytes} \cdot \mathrm{Xfr}\ . \tag{2}$$

Xfr = 10ns/byte or 2.5ns/byte is the data throughput of the cPCI bus for the 32 bit, 33 MHz or 64 bit, 66 MHz operation, respectively. The trigger rearm time is $\leq 25\mu$s. For 8 FADC channels per crate this amounts to a dead time of $\leq 300\mu$s between each two events in in the 64 bit, 66 MHz case.

In the segmented memory mode the available digitizer memory is divided into several segments, each with the length of N sampling points. Each segment is used as a circular buffer. After the trigger the digitizer acquires the N sampling points with the first data point being anywhere in the circular buffer. After this the data are written to the next circular buffer and the trigger is re-armed for the next acquisition. The dead time between two events is as short as ≤ 25ns. This process is repeated until all segments are filled. Only then the CPU reads the data from the digitizer using a single DMA. The total read-out time for M segments is :

$$T_{2a} = \mathrm{Ovhd}_{\mathrm{DMA}} + (N + \mathrm{Extra}) \cdot 2\mathrm{bytes} \cdot \mathrm{Xfr} \ , \tag{3}$$

where Extra ≤ 200 denotes the number of "overhead" data points per segment. After the DMA is terminated the CPU must copy the data from the FADC memory image to a final linear buffer for each segment. For M segments this requires a time of:

$$T_{2b} = M \cdot \mathrm{Ovhd}_{\mathrm{buf}} + M \cdot N \cdot \mathrm{Cpy} \ . \tag{4}$$

where $\mathrm{Ovhd}_{\mathrm{buf}} = (1 \ldots 2)\mu$s is the circular buffer analysis overhead time per segment. Cpy $= (2 \ldots 4)$ns/byte is the time to copy a byte in the FADC RAM. For 8 FADC channels per crate and 100 segments this amounts to a total dead time of ≤ 16ms.

The use of the on-board memory of the FADC as a FIFO offers an effective reduction of dead time through an asynchronous writing of FADC samples data to the FADC memory and transfer to the crate controller PC. It is planned to use the FIFO memory mode as a standard read-out for the FADC multiplexer.

5 Prototype Test in the MAGIC Telescope on La Palma

Two prototype MUX-FADC read-out modules for 32 channels have been tested as a read-out of the MAGIC telescope during two weeks in August/September 2004.

The main goals for the tests were:

- test of concept of the ultra-fast MUX-FADCs under realistic conditions
- study the interplay of the MUX-FADC system with the MAGIC trigger and data acquisition system
- implement the reconstruction and calibration for the ultra-fast digitized signals in the common MAGIC software framework Mars [14]
- provide input for detailed MC simulations for the ultra-fast digitization.

5.1 Setup of the Prototype Test

Two MUX boards of 16 channels each have been integrated into the MAGIC read-out system allowing the simultaneous data taking with the current 300 MSamples/s read-out and the MUX-FADC prototype read-out. Figure 17 shows in a block diagram how the MUX-FADC prototype read-out system has been integrated into the current MAGIC FADC read-out. The analog optical signals arriving from the MAGIC PMT camera are split into two equal parts using fiber optic splitters. One part of the optical signal is connected to the current MAGIC receiver boards which provides output signals to the MAGIC majority trigger logic [15] and to the current 300 MSamples/s FADCs. The other part of the optical signal is delayed by a channel specific delay of 0...15 times 40 ns plus common base delay and directed to the optical receivers on the MUX boards. The common MAGIC trigger is used to trigger the MUX boards as well as the fast FADCs.

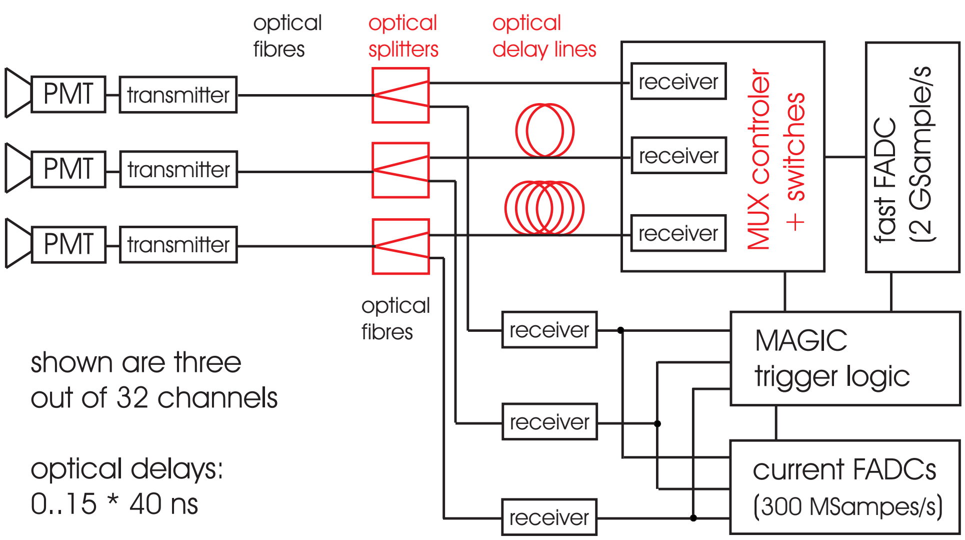

Figure 17: Block diagram of the integration of the MUX-FADC prototype read-out in the current MAGIC FADC read-out. Shower images are simultaneously recorded with the ultra-fast MUX-FADC system and with the current MAGIC FADCs. The MAGIC trigger logic provides a trigger for the MUX electronics as well as for the ultra-fast FADCs.

Figure 18 shows the group of 32 selected channels of the MAGIC PMT camera [4] to be read out by the ultra-fast digitizing system. The channels are chosen to be close packed in order to contain (at least partially) images of showers. In the test 16 bifurcation and 16 GRIN type splitters were used.

In order to acquire only events where the shower image is located in the 32 MUX-FADC channels, only these channels were enabled in the MAGIC trigger system. The trigger fires if the signal in at least four close packed pixels exceeds the preset threshold.

In the prototype tests on La Palma an older version of the ultra-fast FADC has been used, the Acqiris DC240. It features a sampling speed of 2 GSamples/s with an 8 bit resolution. It was connected via a PCI bridge to a host PC running under Windows.

For every trigger 1300 FADC samples (16 times 80 samples plus 20 extra samples) were recorded with both of the used multiplexed FADC channels. An FADC memory of 120 segments was used. In the host PC the data were written into a binary file. This setup was chosen for simplicity and not

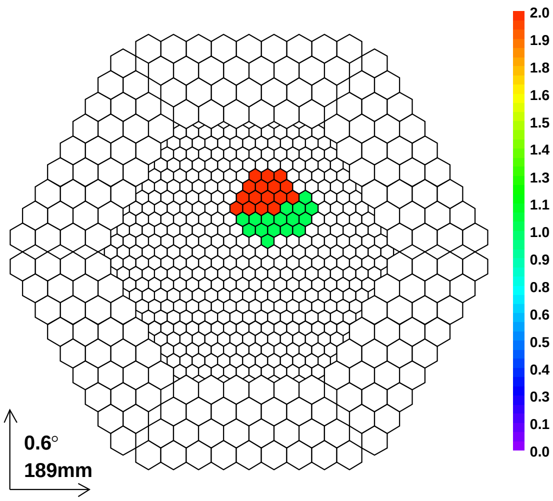

Figure 18: Location of the selected 32 channels in the MAGIC PMT camera.

optimized for the smallest dead time in a continuous data taking mode. Nevertheless the dead time between two of the 120 consecutively recorded events in the segmented mode was negligible.

5.2 Data taken

The tests of the MUX-FADC system have been carried out around the full moon time. In total about 230000 triggers have been taken with the MUX-FADC read-out system (including pedestals and calibration LED light pulses). Table 3 summarizes the amount of data taken with and without the presence of moon light.

trigger type	current FADC read-out	MUX-FADC read-out
pedestals, no moon	500	26400
pedestals, moon	5000	13210
calibration, no moon	47000	96000
calibration, moon	91000	70420
cosmics, no moon	500	8040
cosmics, moon	0	16800
total	144000	230870

Table 3: Overview of the data taken during the MUX-FADC prototype test in the MAGIC telescope at La Palma.

5.3 Data analysis

Each data file contains 120 events of two ultra-fast FADC channels with 1300 recorded FADC samples per event. The recorded raw data are converted into the usual ROOT-based MAGIC raw data format [14], which provides the flexibility to adjust the number of recorded samples for each pixel.

5.3.1 Signal Reconstruction

For each event the signals of 16 PMTs of the MAGIC camera are sequentially digitized by one FADC channel. As an example, figure 19 shows the raw data for 120 superimposed randomly triggered pedestal events. Between two consecutive channels the switch noise is visible. The switch noise is present in less than 10 ns of the recorded 40 ns time interval per read-out channel.

For calibration purposes the MAGIC PMT camera can be uniformly illuminated by a fast LED light pulser located in the center of the telescope dish [16]. Figure 20 shows the raw data of 16 consecutively read-out channels for 120 superimposed calibration events. The calibration signal pulses are clearly visible on the signal baseline. The gain difference from channel to channel is mainly due to a spread in the gain of the VCSEL and receiver diodes of the analog optical link. The additional spread due to small differences in the fiber optic splitters and a signal attenuation in the delay lines is small.

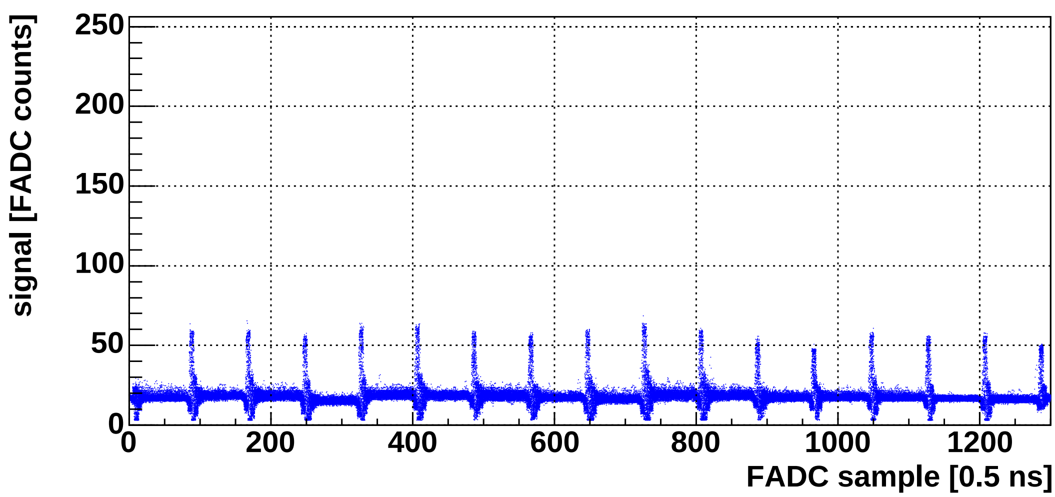

Figure 19: Pedestals: Raw data (1300 samples for 16 consecutive channels) for 120 randomly triggered events overlayed.

For each channel the pedestal level and pedestal RMS are calculated from either a pedestal run with random triggers or directly from the data. For the pedestal calculation a fixed number of FADC samples at a fixed position in the digitization window is used.

For the signal reconstruction a fixed number of FADC samples is integrated. The integration interval is chosen to be 4 FADC samples (corresponding to 4*3.33 ns = 13.33 ns) for the current MAGIC FADCs. For the MUX-FADCs a window size of 10 FADC samples is chosen, corresponding to a 5 ns integration window. The reconstructed signal $\overline{S}$ is then given by:

$$\overline{S} = \sum_{i=i_0}^{i=i_0+3(9)} S_i \ , \tag{5}$$

where S_i is the i-th FADC sample after the trigger. The signal arrival time relative to the first FADC sample after the trigger, t_{arrival}, is reconstructed as the first moment of the FADC time samples used to calculate the reconstructed signal:

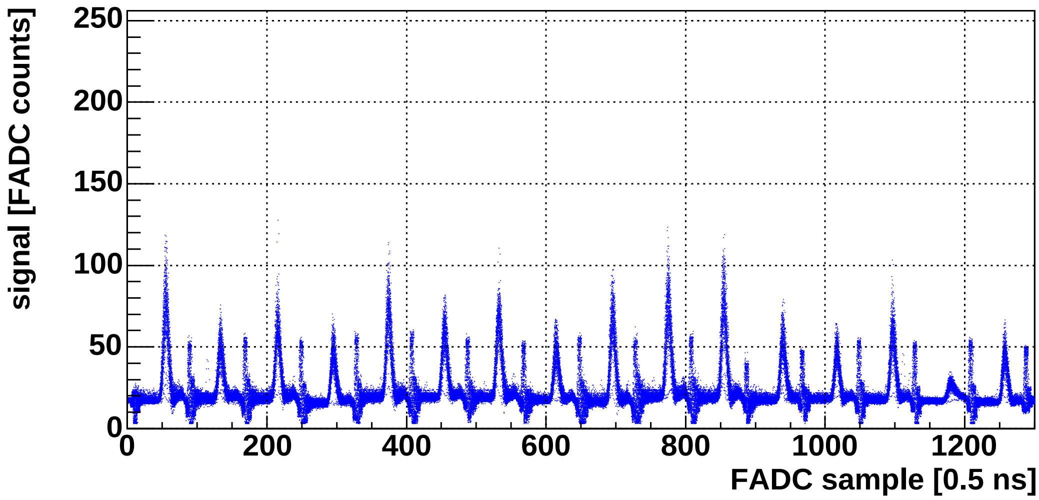

Figure 20: Calibration events: Raw data (1300 samples for 16 consecutive channels) for 120 LED light pulses overlayed.

$$t_{\text{arrival}} = \frac{\sum_{i=i_0}^{i=i_0+3(9)} S_i(t_i - t_{i_0})}{\sum_{i=i_0}^{i=i_0+3(9)} S_i} \ . \tag{6}$$

5.3.2 Calibration

The calibration system of the MAGIC telescope consists of intensity controlled fast LED light pulsers of different colors and intensities that illuminate the MAGIC camera homogeneously [16]. Using the laboratory measured excess noise factor of the MAGIC PMTs the conversion constant between reconstructed signals in FADC counts and photo electrons can be determined. The common MAGIC calibration algorithms and software were successfully applied to the ultra-fast digitization.

Figure 21 shows the distribution of the mean number of photo electrons per pixel reconstructed with the current 300 MSamples/s FADC system and the MUX-FADC system. The MAGIC camera was illuminated with UV calibration pulses. As expected, the mean reconstructed number of photo electrons is the same for the 32 split channels used in the MUX-FADC tests as for all the other MAGIC read-out channels.

Small differences in the cable length of the MAGIC analog optical link, the fiber optic delays and transition times in the PMTs introduce arrival time differences between of the pulses in different read-out channels of up to a few ns. These relative channel to channel time differences can also be calibrated using the LED pulser. One can determine the mean time difference between all pixels with respect to a reference pixel. In the calibration procedure of the cosmics events this timing difference is corrected for.

Moreover, the event to event variation of the timing difference between two read-out channels for the LED pulser provides a measure of the timing accuracy. Figure 22 shows the distributions of the determined timing resolution of the current 300 MSamples/s FADCs together with the timing resolution of the MUX-FADCs. The timing accuracy strongly depends on the signal to noise ratio.

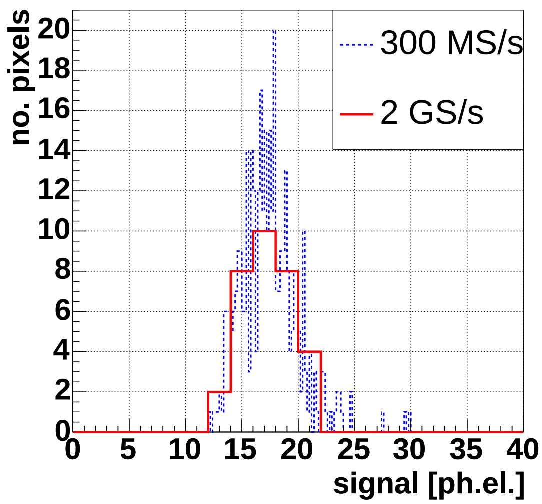

Figure 21: Distributions of the mean reconstructed number of photo electrons in the PMTs of the MAGIC camera from the LED pulser for the current 300 MSamples/s FADCs and the MUX-FADCs. Both read-out systems yield the same average number of photo electrons.

The MUX-FADCs yield a better timing resolution by more than a factor of three compared to the current FADC system.

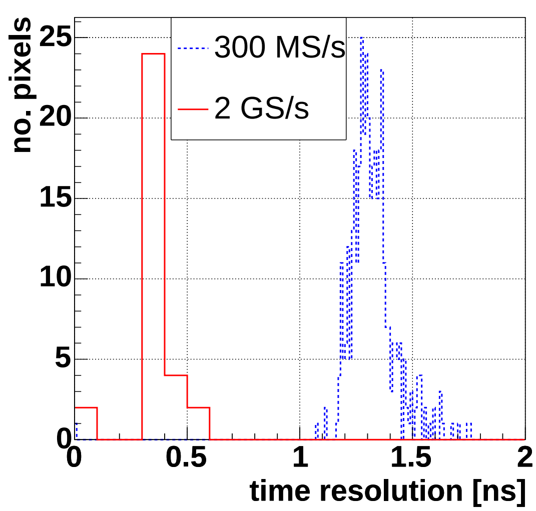

Figure 22: Distributions of the timing resolution for the current 300 MSamples/s FADC read-out and the MUX-FADC read-out. The MUX-FADC system yields an improvement in the timing resolution by more than a factor of three.

5.3.3 Cosmics Data

Cosmics shower data have been recorded to study in detail the interplay of the ultra-fast MUX-FADC system with the MAGIC trigger logic. It also provides valueable input for the MAGIC MC simulations of the ultra-fast digitization system, e.g. about the pulse shapes for cosmics events.

In figure 23a one can see the pulse shape in a single pixel for a typical cosmics event. By overlaying the recorded FADC samples of many events after adjusting to the same arrival time, the average reconstructed pulse shapes can be calculated. Figure 23b shows the comparison of the average reconstructed pulse shapes recorded with the current 300 MSamples/s MAGIC FADCs, including the 6ns pulse stretching, and with the MUX-FADCs. The average reconstructed pulse shape for cosmics events has a FWHM of about 6.3 ns for the current FADC system and a FWHM of about 3.2 ns for the MUX-FADC system.

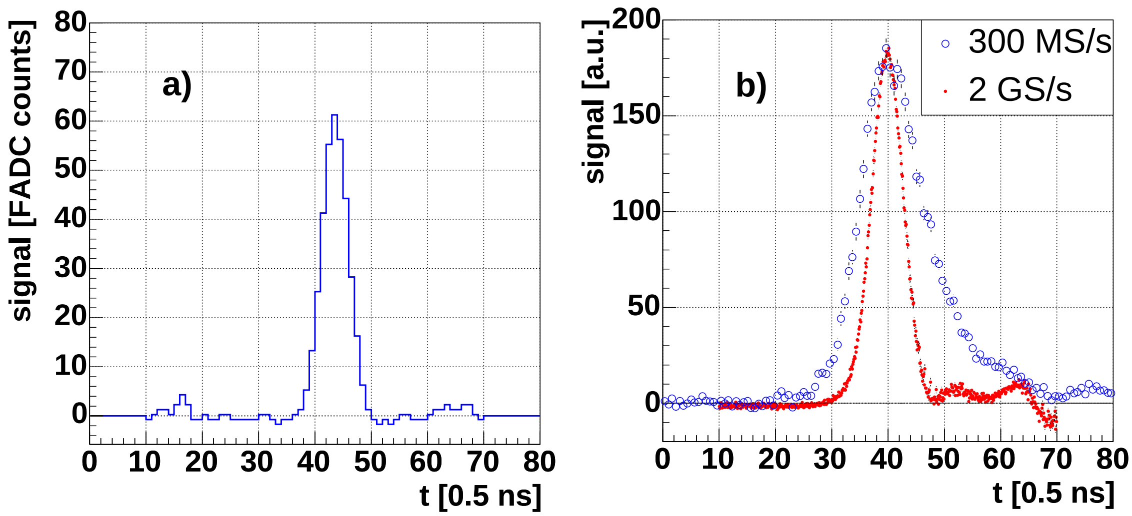

Figure 23: a) Pulse shape in a single pixel for a typical cosmics event after pedestal subtraction. b) Comparison between the mean reconstructed pulse shapes recorded with the current MAGIC FADCs (red triangles) and with the MUX-FADCs (blue circles).

Figure 24a shows a MAGIC PMT camera display with the reconstructed signal after calibration in photo electrons for a typical cosmics event. For the same event figure 24b shows the reconstructed arrival time after correction for the cannel-to-channel time differences.

5.3.4 Pedestals / Noise

In the IACT recorded data the electronics noise together with the LONS fluctuations is superimposed on the Cherenkov signal from showers. The noise from the LONS can be simulated as the superposition of the detector response to single photo electrons arriving at a given rate randomly distributed in time. This can be quantified using the noise autocorrelation function $\boldsymbol{B_{ij}}$, the correlation between the read-out samples i and j:

$$\boldsymbol{B_{ij}} = \langle b_i b_j \rangle - \langle b_i \rangle \langle b_j \rangle \ , \tag{7}$$

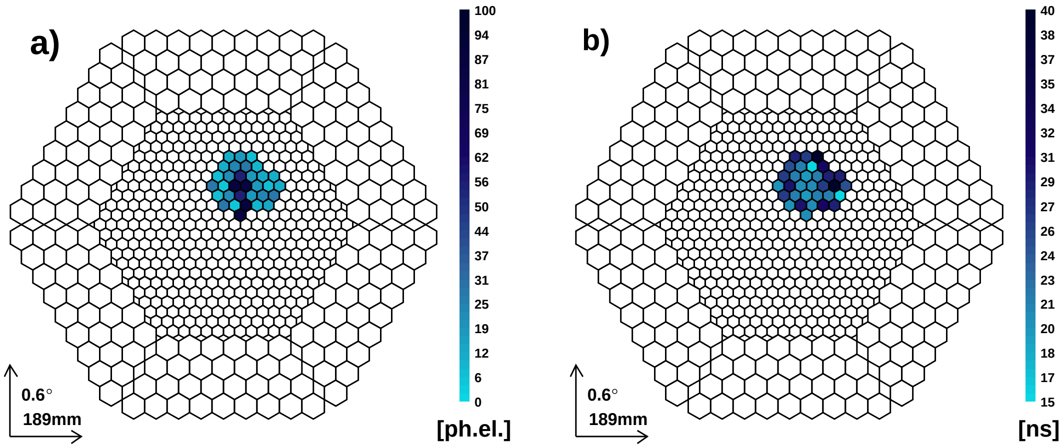

Figure 24: a) Reconstructed signal in photo electrons in the MAGIC PMT camera display and b) calibrated arrival times in ns in the MAGIC camera display for a typical cosmics event.

where b_i and b_j are the FADC samples i and j for a pedestal event.

Figure 25 shows the noise autocorrelation for the current MAGIC FADC system and the MUX-FADC system with open camera, normalized to the pedestal RMS. In the same plot, the noise autocorrelation for the MUX-FADC system with closed camera, normalized to the pedestal RMS for an open camera, is shown. The noise autocorrelation of the current FADC system extends to several ns since the pulse is stretched by 6 ns. For the MUX-FADC system with no intentional pulse shaping there is still a considerable noise autocorrelation for an open camera. A substantial part of the noise is due to the PMT response to the LONS. The noise autocorrelation mostly disappears in case of a closed camera with electronics noise only.

Figure 26 shows the distributions of the mean noise after calibration in photo electrons for the current FADC system and for the MUX-FADC system. The shorter integration time used for the pulse reconstruction with the MUX-FADC system yields a reduction of the effective integrated noise by about 40%. This shall allow us to reduce the analysis energy threshold for Cherenkov images.

Using the new MUX-FADC system the noise contributions due to the LONS may even be resolved into individual pulses. Figure 27 shows a typical example for the signals in a pedestal event (random triggers). The pedestal does not vary in an uncorrelated way. Instead most of the pedestal variations are due to "bumps" on the signal baseline.

The rate of the bumps has been studied to varify whether it is compatible with the rate of LONS photo electrons. A window of 6 slices is slid over the FADC samples of randomly triggered pedestal events. The first window position after the switch noise where the sum of the FADC samples exceeds the pedestal level by at least 3 FADC counts was chosen. Figure 28a shows the arrival time distribution of the first noise "bump". The distribution can be fit by an exponential function with a rate r of

$$r = (0.13 \pm 0.01)\mathrm{ns}^{-1} \ . \tag{8}$$

This corresponds to an integrated noise of about 1.3 photo electrons per 10 ns integration window,

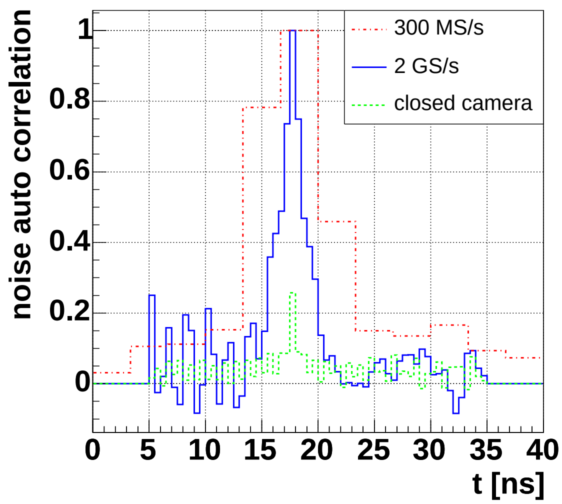

Figure 25: Noise autocorrelation function with respect to a fixed FADC sample for the current MAGIC readout chain with 6 ns pulse shaping, the MUX-FADC read-out with open camera and closed camera, normalized to the pedestal RMS of the opened camera.

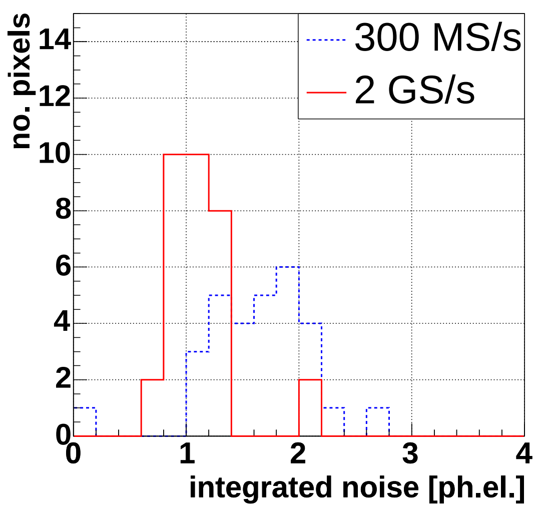

Figure 26: Distributions of the integrated noise in the signal reconstruction window after calibration into photo electrons for the current 300 MSamples/s FADC read-out and using the MUX-FADC read-out.

which is in good agreement with the expected LONS rate.

Figure 28b shows the pulse shape of the selected noise "bumps" averaged over many events. The mean charge of the noise "bump" corresponds within errors to the mean charge for a single photo electron. Due to the amplitude resolution of 8 bit in the test setup it is still quite difficult to resolve the single photo electrons due to the LONS. With the higher resolution of 10 bit with the full MUX-FADC

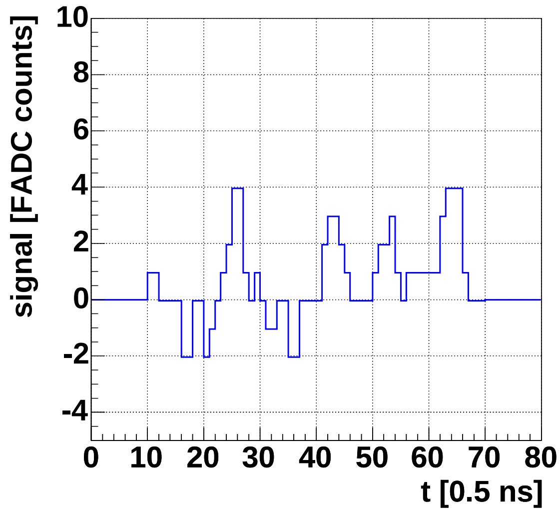

Figure 27: Time structure in a typical pedestal event. The bumps on the baseline might be due to single photo electrons from the light of the night sky.

system even a continuous calibration of the read-out chains using the single photo electrons shall be possible.

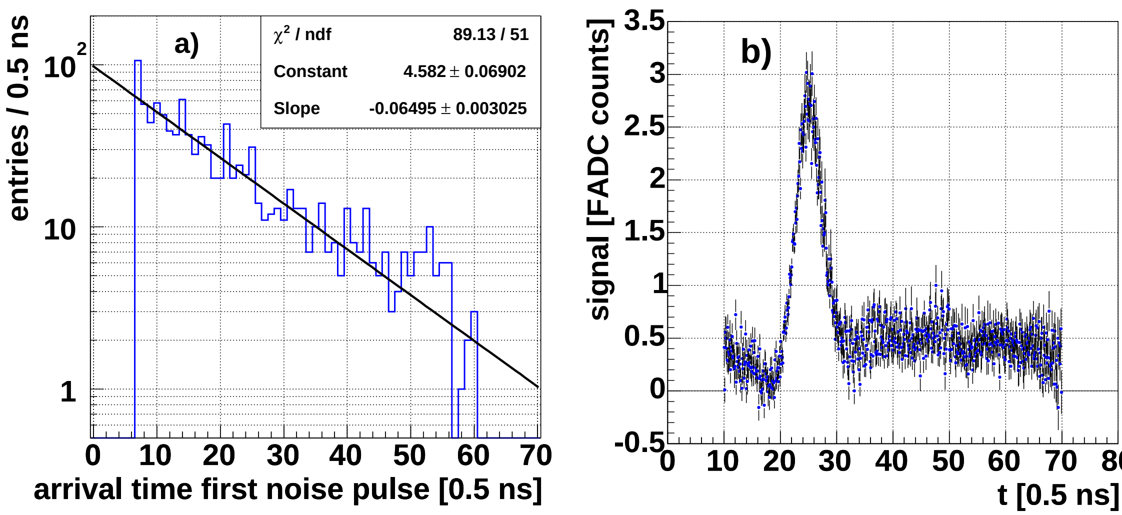

Figure 28: a) Arrival time distribution of the first "bump" on the pedestal baseline. The bumps are arriving randomly in time with a rate of $(0.13 \pm 0.01)\mathrm{ns}^{-1}$. b) Average reconstructed shape of the LONS noise "bumps".

5.3.5 MC Simulations

The response of the MAGIC telescope to gamma ray showers and to background has been simulated in detail [17]. Both the currently used 300 MSamples/s readout chain and the ultra-fast digitization have been simulated.

Figure 29 shows the reconstructed single photo electron spectrum of a simulated pedestal run. The highest integral of 8 FADC slices (4 ns) has been searched for in a fixed 20 slices (10 ns) digitization window. The left peak corresponds to and electronics noise only. The right part of the distribution corresponds to the response of the PMT to one or more photo electrons.

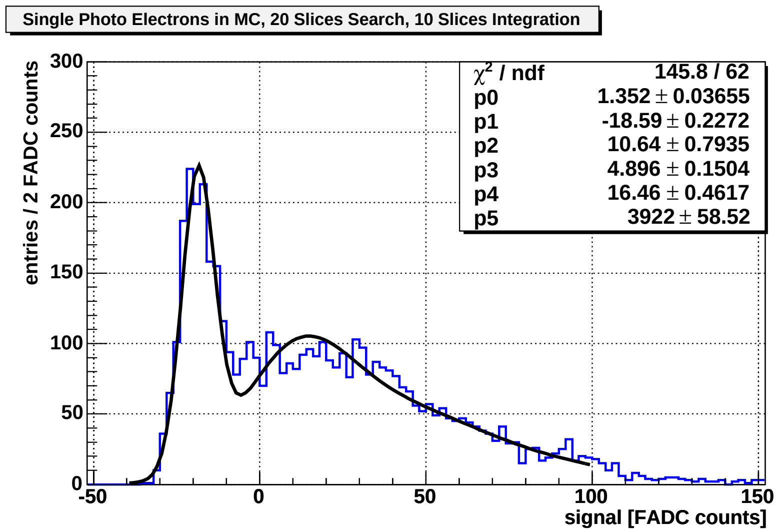

Figure 29: Reconstructed single photo electron spectrum of a simulated pedestal run. The left peak is the pedestal.

In figures 30 the signal and arrival time resolutions which can be achieved with the current and the MUX-FADC system are compared using MC simulations. For both MC simulations the same night sky background conditions are assumed as well as the same electronics noise level. Figure 30a shows the resolution of the reconstructed pulse arrival time as a function of the input signal. The MUX-FADC system improves the timing resolution by more than a factor of 3. This is compatible to the results in the data. Figure 30b shows the resolution of the reconstructed charge as a function of the input charge. With the MUX-FADC system the charge resolution improves by a factor of two.

6 Discussion

The ultra-fast fiber-optic multiplexed FADC prototype read-out system has successfully been tested during normal observations of the MAGIC telescope in La Palma. The fiber-optic splitters and delays are commercially available and comply with the required specifications for the use in the ultra-fast MUX-FADC read-out system. The 10 bit 2 GSamples/s FADCs from Acqiris are developed for MAGIC and available now as a commercial product. Thus the ultra-fast FADC read-out has grown to a mature technology which is ready for the use as a standard read-out system of the MAGIC telescope and other high-speed data acquisition applications.

The multiplexing of 16 channels into one ultra fast FADC allows one to greatly reduce the price of an ultra-fast read-out system. The MUX-FADC read-out reduces the costs by about 85% compared to using one ultra-fast FADC channel per read-out channel. Also the power consumption of the read-out system is greatly reduced.

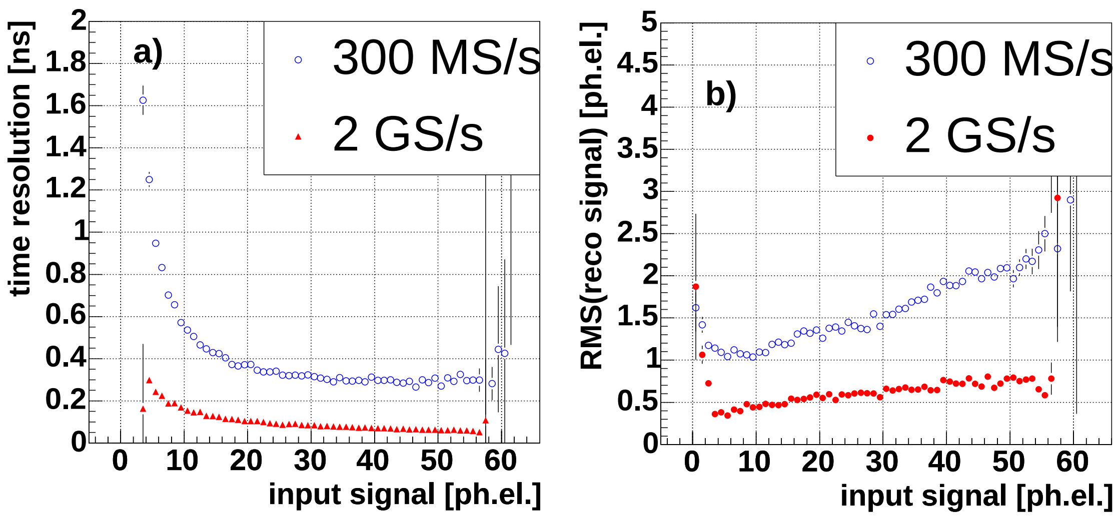

Figure 30: a) Comparison of the pulse arrival time resolution as a function of the input signal size between the current MAGIC 300 MSamples/s FADCs and the 2 GSamples/s FADCs. The time resolution improves by more than a factor of 3 with the new system. b) Comparison of the signal resolution as a function of the input signal with the current 300 MSamples/s MAGIC FADCs and the 2 GSamples/s FADCs system. The signal resolution improves by a factor of about two.

Through the use of a smaller integration window of the Cherenkov pulses less noise due to fluctuations of the LONS is integrated. For the used integration windows of 13.33 ns for the current MAGIC FADC system and 5 ns for the MUX-FADC system this corresponds to a reduction in noise of about 40%. Thus the image quality of the Cherenkov showers will improve with the ultra-fast read-out system. This will allow the reduction of the analysis energy threshold of the MAGIC telescope.

Moreover the ultra-fast FADC system provides a greatly improved resolution of the timing structure of the shower images. As indicated by MC simulations gamma showers, cosmic ray showers and the so called single muon events have different timing structures. Thus the ultra-fast FADC read-out can enhance the separation power of gamma showers from backgrounds.

7 Outlook: MagicII MUX-FADC read-out

After the successful prototype test of the ultra-fast MUX FADC read-out system it is considered as a future read-out option of the MAGIC telescope. Figure 31 shows the proposed mechanical arrangement of the full MUX-FADC read-out system for the MAGIC telescope. It consists of 7 racks:

- one DAQ and data storage rack
- one rack for the trigger logic, use of the current MAGIC trigger electronics
- one trigger receiver rack, use of the current MAGIC receiver boards with adjustable discriminator thresholds
- four racks containing the optical splitters and delays, the MUX electronics and the FADCs.

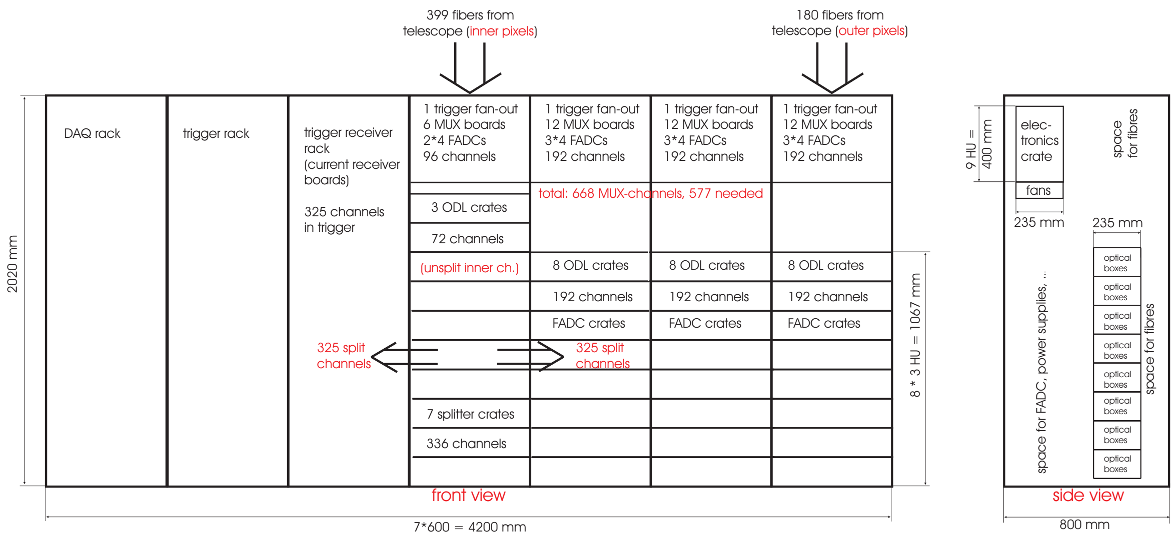

Figure 31: Mechanical Arrangement of the MUX-FADC read-out system.

Only the 325 inner-most pixels of the MAGIC PMT camera are used for the majority trigger logic [15]. Thus only for these channels part of the analog optical signal has to be split off before the delay fiber to initiate the trigger decision.

A possible setup of the DAQ system consists of 5 FADC crates with fast crate controller PCs which are connected via Gbit/s Ethernet with a host PC. In the host PC the FADC data corresponding to one event are merged together and some auxiliary data like an accurate event time information are added. The host PC controls a fast RAID system for data storage.

The high trigger rate in conjunction with the large read-out data per event represents a challenge for the DAQ system. For each event 80 samples per 2 bytes have to be read-out. For 600 channels this amounts to a total event size of about 96 kbytes per event. Assuming a maximum maintained trigger rate of 1 kHz this corresponds to a data rate of nearly 100 Mbytes/s or 2 to 3 TByte per night.

To reduce the data amount it is planned to cut out part of the data which is affected by the MUX-switching on the crate controller level. A further data reduction is planned after the event building on the host PC through a software compression. As the data storage space on the RAID is limited the data has to be transferred to tapes during the non-observation times.

The implementation of the ultra-fast digitized data into the common MAGIC software framework and MC simulations will provide a minimum transition time from the current MAGIC FADC read-out system to the ultra-fast MUX-FADC read-out system.

A Acknowledgements

The authors thank R. Maier and T. Dettlaf from the electronics work shop of MPI for the layout, design and production of the MUX-FADC electronics. Moreover the very good collaboration with the companies Acqiris and Sachsenkabel is acknowledged.

References

[1] E. Lorenz, *Very High Energy Gamma Ray Astronomy*, Nucl.Phys.B (Proc.Suppl.) **114** (2003) 217.

[2] J. A. Barrio (MAGIC Collab.), *The MAGIC Telescope - Design Study for the Construction of a 17m Cherenkov Telescope for Gamma Astronomy above 10 GeV*, MPI-PhE-98-05.

[3] J. Cortina et al. (MAGIC Collab.), *The data acquisition of the MAGIC telescope*, Prepared for International Symposium: The Universe Viewed in Gamma Rays, Kashiwa, Chiba, Japan, 25-28 Sep 2002.

[4] C. Baixeras et al. (MAGIC Collab.), *Commissioning and first tests of the MAGIC telescope*, Nucl. Instrum. Meth. **A518** (2004) 188.

[5] S. Commichau, private communication.

[6] D. Mazin et al., *Shower templates for the MAGIC Telescope*, In preparation .

[7] A. Ostankov et al., *A study of the new hemispherical 6-dynodes PMT from electron tubes*, Nucl. Instrum. Meth. **A442** (2000) 117.

[8] E. Lorenz et al., *A fast, large dynamic range analog signal transfer system based on optical fibers*, Nucl. Instrum. Meth. **A461** (2001) 517.

[9] R. Mirzoyan et al., *Ultrafast FADC Multiplexer*, IEEE Trans. Nucl. Sci. **49** (2002) 2473 .

[10] R. Mirzoyan, J. Cortina, and E. Lorenz, *Multiple Signal Channel Read Out by a Single FADC*, Prepared for 27th International Cosmic Ray Conferences (ICRC 2001), Hamburg, Germany, 7-15 Aug 2001.

[11] J. Lipson and G. Harvey, *Low-loss wavelength division multiplexing (WDM) devices for single-mode systems*, Journal of Lightwave Technology **1** (1983) 387.

[12] *Sachsenkabel GmbH*, `http://www.sachsenkabel.de`.

[13] *Acqiris SA*, `http://www.acqiris.com`.

[14] T. Bretz and R. Wagner (MAGIC Collab.), *The MAGIC analysis and reconstruction software*, Prepared for 28th International Cosmic Ray Conferences (ICRC 2003), Tsukuba, Japan, 31 Jul - 7 Aug 2003.

[15] M. Meucci et al. (MAGIC Collab.), *The trigger system of the MAGIC telescope: On-line selection strategies for Cherenkov telescopes*, Nucl. Instrum. Meth. **A518** (2004) 554.

[16] T. Schweizer et al., *The optical calibration of the MAGIC telescope camera*, IEEE Trans. Nucl. Sci. **49** (2002) 2497.

[17] A. Moralejo et al., *MC Simulations for the MAGIC Telescope*, In preparation .